Editors' Suggestion

Ultimate Accuracy of Frequency to Power Conversion by Single-Electron Injection

Jukka P. Pekola,[1] Marco Marín-Suárez,[1] Tuomas Pyhäranta,[1] and Bayan Karimi[1,2]
[1]Pico group, QTF Centre of Excellence, Department of Applied Physics, Aalto University, P.O. Box 15100, FI-00076 Aalto, Finland
[2]QTF Centre of Excellence, Department of Physics, Faculty of Science, University of Helsinki, FI-00014 Helsinki, Finland

(Received 18 April 2022; revised 14 June 2022; accepted 15 June 2022; published 12 July 2022; corrected 13 January 2023)

We analyze theoretically the properties of the recently introduced and experimentally demonstrated converter of frequency to power. The system is composed of a hybrid single-electron box with normal island and superconducting lead, and the detector of the energy flow using a thermometer on a normal metal bolometer. Here, we consider its potential for metrology. The errors in power arise mainly from inaccuracy of injecting electrons at the precise energy equal to the energy gap of the superconductor. We calculate the main systematic error in the form of the excess average energy of the injected electrons and its cumulants, and that due to subgap leakage. We demonstrate by analytic and numerical calculations that the systematic error in detection can, in principle, be made much smaller than the injection errors, which also, with proper choice of system parameters, can be very small, $< 1\%$, at low enough temperature. Finally, we propose a simplified configuration for metrological purposes.

DOI: 10.1103/PhysRevLett.129.037702

Single-electron and superconducting devices form important building blocks in modern electrical metrology. Voltage from the Josephson effect, resistance from the quantum Hall effect and current from single-electron transport are all reliable ways to determine these quantities with high accuracy [1–5]. Extending to other application areas of quantum electronic devices [6,7], some of us have recently demonstrated a hybrid single-electron transistor as a frequency to power converter [8,9]. In this first experiment the accuracy in generating a desired level of power was still modest, on the level of about 10%, mainly because of the nonoptimized calibration of the bolometric detector. In this Letter we discuss the fundamental errors of the frequency to power conversion arising from nonadiabaticity, noise, subgap leakage, and temperature. Similarly, we analyze the error of the bolometric detector in the form of trapping efficiency of the absorber whose temperature is monitored. The injector and detector form an all-in-one system compatible for integrated design and fabrication, schematically depicted in the center of Fig. 1. We obtain analytical results that allow for direct assessment of experimental opportunities, and propose a simplified setup for future precision experiments.

The heart of the system is a single-electron emitter (NIS electron box; N for normal metal, I for insulator, S for superconductor), see Fig. 1. The key idea is that periodically varying gate voltage, at frequency f, one injects electrons between the N island and the S lead at an energy close to the superconducting gap Δ. In the first demonstration (Ref. [8], see also [10]) a variation of this setup was employed demonstrating power P output close to $2f\Delta$. We denote the time-dependent chemical potential of the N island with respect to the S lead by v (in units of Δ), modulated by the gate voltage. The given result, $P \approx 2f\Delta$ into S, is easy to understand by noting that the Bardeen-Cooper-Schrieffer (BCS) density of states (DOS) in the superconductor [13] vanishes at subgap energies and has a singularity at the gap. Therefore, under the gate drive with not too high frequency, the electrons indeed tunnel very

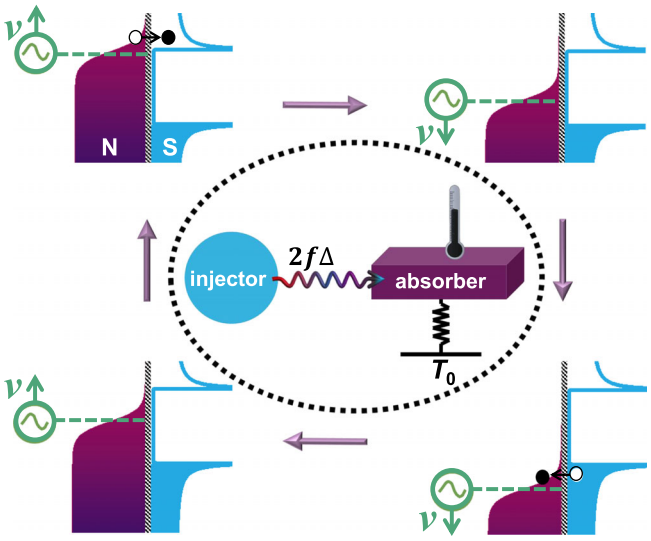

FIG. 1. The pumping cycle to convert frequency to power. The potential of the normal (N) electron box is shifted periodically by the gate voltage v with respect to that of the superconducting lead (S). Each time the N potential passes the gap energy in S, an electron tunnels to and from N creating an excitation with energy $\sim\Delta$. In the center we illustrate the all-in-one system consisting of the power injector and absorber whose temperature is then measured.

close to the gap energy of the superconductor. The cycle leading to the given value of power is illustrated by the cartoon in Fig. 1. Systematic errors in injection energy, and thus average power over many driving periods, arise from the delayed on-demand tunneling events if the gate voltage passes the singularity condition too fast, and from fluctuations of the same effect. In the analysis below we also take into account the nonvanishing temperature T, and nonidealities in tunneling.

Besides injection, errors in f to P conversion can incur due to the detection of P, which is done bolometrically. The excitations, electronlike or holelike quasiparticles in the superconductor, diffuse through the superconducting wire into a normal metal absorber, and the power is measured by detecting the steady-state rise of the temperature of this N absorber [14]. Fundamental errors arise due to the loss of quasiparticle energy to phonons [15] or via the leakage of heat through the whole SNS chain around the absorber in the diffusion process [16], and due to the error of the temperature measurement.

Optimal operation of the frequency to power conversion is achieved at low temperature ($k_B T \ll \Delta$), at moderately low frequencies, and with nearly ideal junctions. In this case most of the results of interest can be obtained analytically with illustrative and characteristic results demonstrating the scaling of errors in terms of device parameters, driving frequency, and temperature. Eventually, we present both analytic and numeric results with good consistency. The numerical analysis follows closely that presented in Ref. [8] but extended to higher moments of injected energy, see Supplemental Material [10].

For small errors we make first the following Markovian assumption: the deposited energy in a pumping cycle (one event in each half-period, see Fig. 1) is assumed to be independent of the history. This is justified by the fact that, with high accuracy, the system is reset to the desired charge state after each half-period. We also assume that back-tunneling is sufficiently weak, meaning that only one favorable tunnel event occurs near the matching condition of island potential v (in units of Δ) and the gap in the lead. Therefore, we obtain the average power and its cumulants by focusing on the rising part of $v(t)$, and solve the master equation $dp/dt = -\Gamma(t)p(t)$, where $p(t)$ is the survival probability of the charge on the island with formal solution $p(t) = p(0)e^{-\int_0^t d\tau\Gamma(\tau)}$. The rate out when the island is gate biased at v reads $\Gamma = (\Delta/e^2R_T)\int d\epsilon\, n_S(\epsilon)f_N(\epsilon - v)\times [1 - f_S(\epsilon)]$. Here, R_T is the tunnel junction (normal state) resistance, $f_X(\epsilon) = 1/(1 + e^{\beta_X\epsilon})$ is the Fermi-Dirac distribution of electrons on the $X = N$, S electrode at inverse $\beta_X = \Delta/(k_B T_X)$ of the temperature T_X, and $n_S(\epsilon)$ is the BCS DOS in the superconductor [13]. The energies are here normalized by Δ, so that $n_S(\epsilon) = 0$, when $|\epsilon| \le 1$, and $|\epsilon|/\sqrt{\epsilon^2 - 1}$ otherwise.

With no subgap tunneling, we have $\Gamma = 0$ at $v < 1$. At gate biases above the gap ($v > 1$), we obtain the zero temperature rate as $\Gamma = (\Delta/e^2R_T)\sqrt{v^2 - 1}$. We assume a linear ramp $v = \dot{v}t$ in time t, where $\dot{v}$ is the constant rate of change of v. Such a choice is generally valid since tunneling mainly occurs around the singularity of the BCS DOS, i.e., when $|v| \approx 1$. This $\dot{v}$ is proportional to the frequency f for a given waveform of pumping. With no subgap tunneling, we have $p = 1$ at $v \le 1$. At gate biases above (but close to) the gap ($v \gtrsim 1$), we obtain the zero temperature survival probability as $p(v) = \exp\{-(1/2\Omega)[v\sqrt{v^2 - 1} - \ln(v + \sqrt{v^2 - 1})]\} \approx \exp[-(2\sqrt{2}/3)\Omega^{-1}(v - 1)^{3/2}]$. Here, $\Omega \equiv e^2R_T\dot{v}/\Delta$ is the dimensionless frequency, which depends also on the system parameters R_T and Δ. To find the statistics of heat in this configuration we write the probability distribution as $P(\epsilon, v) = -p'(v)\Pi(\epsilon, v)$. Here, $\Pi(\epsilon, v)$ is the probability (density) of tunneling to the state with energy ϵ in S, provided it happens at voltage v, given by $\Pi(\epsilon, v) = \pi(\epsilon, v)/\int \pi(\epsilon', v)d\epsilon'$, where $\pi(\epsilon, v) = n_S(\epsilon)f_N(\epsilon - v)[1 - f_S(\epsilon)]$ is the spectral rate at energy ϵ when biased at v. We then obtain the moments of the transmitted energy as $\langle E^n\rangle = \Delta^n \int dv \int d\epsilon\, \epsilon^n P(\epsilon, v)$. We analyze the lowest moments at zero temperature analytically as a power series of Ω. In the lowest order we obtain

$$\frac{\langle E\rangle}{\Delta} = 1 + \frac{\Gamma(2/3)}{3^{4/3}}\Omega^{2/3} \approx 1 + 0.313\ \Omega^{2/3}, \tag{1}$$

where $\Gamma(x)$ is the gamma function. Naturally, the average energy exceeds Δ since the minimum that the tunneling can bring equals Δ. We also calculate the cumulants $\langle \delta E^n\rangle \equiv \langle (E - \langle E\rangle)^n\rangle$. In particular, the standard deviation of the deposited energy is given by

$$\frac{\sqrt{\langle \delta E^2\rangle}}{\Delta} = \left(\frac{3}{2\sqrt{2}}\right)^{2/3}\sqrt{\frac{\Gamma(7/3)}{5} - \frac{\Gamma(5/3)^2}{9}}\Omega^{2/3} \approx 0.400\ \Omega^{2/3}. \tag{2}$$

Similarly, for the cubic root of the third cumulant we have $\sqrt[3]{\langle \delta E^3\rangle}/\Delta \approx 0.520\ \Omega^{2/3}$. The skewness related to the third cumulant is thus always positive.

Besides the influence of driving frequency, deviations from the ideal $P = 2f\Delta$ arise from temperature-independent subgap leakage and from nonvanishing temperature that were ignored above. For the first one, we assume the standard Dynes form of the DOS [17,18] $n_S(\epsilon) = |\mathrm{Re}[(\epsilon + i\gamma)/\sqrt{(\epsilon + i\gamma)^2 - 1}]|$, with the dimensionless smearing parameter γ, which can be directly related to experimental parameters [19]. To obtain the average heat in a half-period, we follow the same procedure as before, but now with the subgap DOS $n_S(\epsilon) \approx \gamma/(1 - \epsilon^2)^{3/2}$ for $|\epsilon| < 1$ and subsequent survival

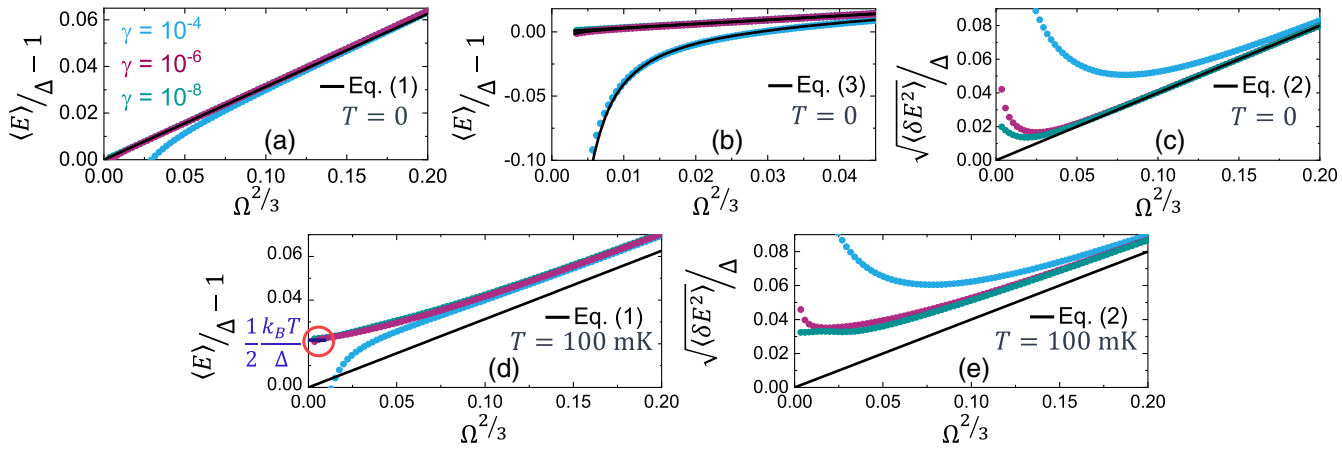

FIG. 2. Main results of the numerical and analytical calculations. In (a)–(c), the results at zero temperature are shown against the dimensionless ramp rate Ω. (a) The average extra energy with respect to Δ. The dependence $0.313\ \Omega^{2/3}$ from Eq. (1) (solid line) closely follows the numerical result. The legend gives the values of the Dynes leakage parameter γ. (b) Close-up of the low Ω regime of (a), together with analytical predictions of Eq. (3) shown by solid lines. (c) Root-mean-square value of the deposited energy presented as in (a) with the solid line from Eq. (2). (d),(e) Average excess energy and its root-mean-square value at nonvanishing temperature, chosen to be $T = 100$ mK with aluminum, $\Delta/k_B = 2.3$ K, for practical comparison. The labels of the symbols and lines are as in (a) and (c). The circle at $\Omega = 0$ in (d) points to the equipartition result of Eq. (4), in full agreement with the numerics for lowest γ as $\Omega \to 0$.

probability $p(1) = e^{-\gamma/\Omega}$. With these we obtain the zero-temperature average heat as

$$\frac{\langle E\rangle}{\Delta} \approx \left(\frac{\pi}{2} - 1\right)\frac{\gamma}{\Omega}e^{-\gamma/\Omega} + (1 + 0.313\ \Omega^{2/3})e^{-\gamma/\Omega}, \quad (3)$$

which coincides with Eq. (1) for $\gamma \to 0$. Naturally, the influence of nonvanishing γ is to lower $\langle E\rangle$ due to tunneling events below the gap.

For the nonvanishing temperature, we return to the ideal BCS DOS to obtain the leading error at low Ω and vanishing γ. Again with the same procedure as above, we find the survival probability at $v = 1$ as $p(1) \approx e^{-\sqrt{\pi/2}\Omega^{-1}(k_BT/\Delta)^{3/2}}$. Therefore, for $\Omega \ll \sqrt{\pi/2}(k_BT/\Delta)^{3/2}$, the tunneling mainly occurs already at $v < 1$ but at energy just above the gap due to the tail in the Fermi-Dirac distribution in N. With standard integrations, this yields the result at $\Omega \to 0$ as

$$\frac{\langle E\rangle}{\Delta} \approx 1 + \frac{1}{2}\frac{k_BT}{\Delta}, \qquad \Omega, \gamma \to 0, \quad (4)$$

presenting an equipartitionlike excess energy in this quasistatic process.

Figure 2 presents the main characteristics of the injector performance. We observe that the numerical results for the two quantities agree quantitatively with the predictions (1) and (2) for $T = 0$ and the smallest γ ($= 10^{-8}$). For nonvanishing leakage, Eq. (3) yields a decent approximation which deviates from the linear behavior especially at low values of Ω [see Fig. 2(b)]. Likewise, the prediction of Eq. (4) captures the quasistatic excess energy toward $\Omega = 0$ at nonvanishing temperatures. We conclude that Eqs. (1)–(4) form a perfect basis of assessing the errors in frequency-to-power conversion.

Next, we analyze the bolometer efficiency and its noise. In the structure of Fig. 3(a), the lead into which the excitations are injected is composed of three sections $S1$ (superconductor), N (normal metal), and $S2$ (superconductor), connected by clean metallic contacts to each other. The section lengths and cross-sectional areas are, respectively, denoted by ℓ_i and A_i with proper subscripts, and the volume of the N absorber is $\mathcal{V}_N$. By combining the continuity equation with Fourier's law, we can derive a one-dimensional model for heat transport. In this model, the temperature difference obeys a nonlinear differential equation of the form

$$\frac{d}{dx}\left[-\kappa(x)A\frac{d}{dx}\theta(x)\right] + \dot{Q}_{\rm ep}(x) = 0, \quad (5)$$

in each of the three regions, with $\theta(x) = T(x) - T_0$ the local temperature with respect to that of the bath, T_0. The problem satisfies the following boundary conditions: (i) heat current into the $S1$ wire on the left end equals P (approximately $2f\Delta$ in practice), (ii) the temperature is continuous across the SN interfaces, (iii) similarly, the heat current is continuous in these interfaces, and (iv) temperature at the right end of $S2$ equals T_0 since this end is intentionally thermalized to the phonon temperature by a big reservoir. Both the thermal conductivity $\kappa(x)$ as well as the power transfer per unit length due to the electron-phonon interaction $\dot{Q}_{\rm ep}(x)$ depend on temperature. For the superconducting regions $\kappa_S = (2\Delta^2/e^2\rho T_S)e^{-\Delta/k_BT_S}$ [20]

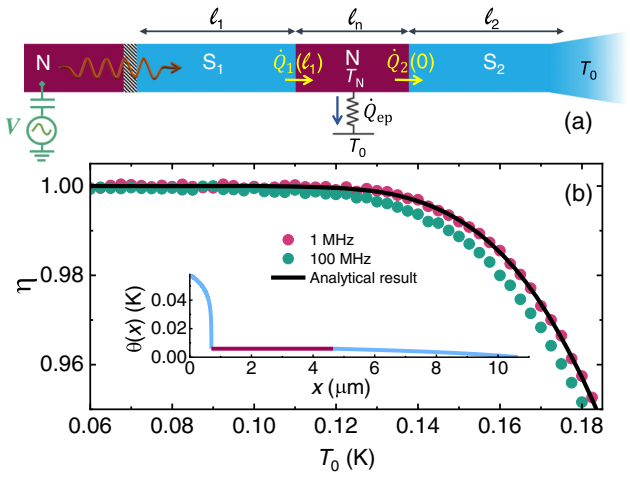

FIG. 3. The bolometric detector. (a) The scheme. The power injected to the superconductor $S1$ diffuses into the normal absorber N and leaks partly to the second superconductor $S2$ which is thermalized to bath temperature T_0 at the far end. (b) Trapping efficiency η as a function of T_0. The numerical results shown by solid symbols are calculated with two injection frequencies. The line is from Eq. (8). The device parameters can be found in [10]. Inset: temperature profile along the structure with coordinate x in (a) with the following parameters: P corresponds to $f = 10$ MHz and $T_0 = 100$ mK, the geometric and material parameters are as in the main panel.

and $\dot{Q}_{\mathrm{ep},S} = a\Sigma_S A_S T_0^4 e^{-\Delta/k_B T_S}\theta(x)$ as derived from [21]. Here, ρ is the normal state resistivity of the superconductor, Σ_S its material specific electron-phonon coupling parameter, and $a \sim 5$ is a numerical constant. For the normal metal the heat conductance is given by the Wiedemann-Franz law and $\dot{Q}_{\mathrm{ep},N} = \Sigma_N A_N[T_N^5(x) - T_0^5]$ with Σ_N the electron-phonon parameter for the normal metal [14]. The inset of Fig. 3(b) depicts a typical numerical solution of the temperature difference along the SNS wire.

For small temperature differences, $\theta(x)/T_0 \ll 1$, valid for low-frequency operation or high bath temperatures, we may neglect the nonlinearities, and Eq. (5) yields approximately

$$\theta''(x) - \lambda^2\theta(x) = 0, \tag{6}$$

where $\lambda = \sqrt{a\Sigma_S e^2\rho/(2\Delta^2)}T_0^{5/2}$. In Secs. $S1$ and $S2$ we solve Eq. (6) whereas in N we assume a constant temperature T_N throughout because of the good thermal conductivity in it [see the normal-metal section of plot in the inset of Fig. 3(b)]. This procedure allows one to solve analytically the temperature profile in the SNS wire for a given set of parameters including P, T_0 and the geometric and material parameters. Our prime interest is to find the trapping efficiency η of the bolometer, which is the ratio of the power absorbed in N and the injected power, i.e., $\eta = \dot{Q}_N/P$ with $\dot{Q}_N = \dot{Q}_1(\ell_1) - \dot{Q}_2(0)$, the difference of incoming and outgoing heat fluxes at the ends of the two

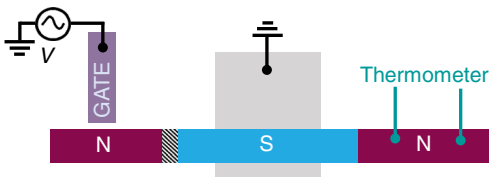

FIG. 4. Proposed improved configuration of the power source. The potential of the S lead is kept fixed by a large capacitance to ground.

superconductors at the intersection with N, see Fig. 3(a). We find then in this linearized model

$$\eta = \frac{\mathrm{sech}\lambda\ell_1}{1 + \varpi(A_1\tanh\lambda\ell_1 + A_2\coth\lambda\ell_2)T_0^{-5}e^{-\Delta/k_BT_0}}, \tag{7}$$

with $\varpi = 2\lambda\Delta^2/(5e^2\rho\Sigma_N\mathcal{V}_N)$. We find for aluminum superconductor at $T_0 = 100$ mK that $\lambda \sim 10^2$ m^{-1}, meaning that the phonon relaxation length is about 1 cm. Then for the typical structure with $\ell_i \ll 100$ μm, $\lambda\ell_i \ll 1$, and Eq. (7) can be approximated to a good accuracy by

$$\eta \approx \left(1 + \frac{\varpi A_2}{\lambda\ell_2}T_0^{-5}e^{-\Delta/k_BT_0}\right)^{-1}. \tag{8}$$

A comparison between the numerical results and the prediction of Eq. (8) is presented in the main panel of Fig. 3(b). We can see that the differences are negligible especially for small frequencies.

Equation (7) demonstrates that the main source of reduced efficiency is the leakage of heat through superconductor $S2$. To suppress this effect one may increase the length ℓ_2, which according to Eq. (8) decreases this leakage-induced loss efficiently. To improve the setup further we propose a configuration as sketched in Fig. 4, where we drop $S2$ out completely. This way the efficiency improves into

$$\eta \approx \mathrm{sech}\lambda\ell_1, \tag{9}$$

determined ideally only by the electron-phonon leakage in $S1$. In this configuration η drops by 0.005% from unity for temperatures around 100 mK and $\ell_1 \lesssim 100$ μm, and exponentially less at lower temperatures.

Finally, we make some practical estimates based on standard materials and experimental constraints. Before that, we note that the systematic error in $\langle E\rangle$ is the same as that in average power, whereas the standard deviation in power diminishes as $\sqrt{\langle\delta E^2\rangle/n}$, where n is the number of pumping cycles averaged in measuring the power. Typically, n is large, $n > 10^6$ for a slow temperature measurement, and therefore the noise in injection can be essentially neglected in comparison to the systematic errors in P. For high quality aluminum-based junctions, γ can be as small as $< 10^{-6}$ [22], which makes its influence quite minor at practical frequencies of operation. Apparently the

temperature error of Eq. (4) is the most fundamental one and hardest to suppress. Using aluminum as the superconductor, $\Delta/k_B \approx 2.3$ K for thin films, and, according to Eq. (4), the error in $\langle E \rangle$ can be made $< 1\%$ if the temperature is $T \lesssim 50$ mK. At the same time one needs to keep the driving frequency $f < 100$ MHz based on Eq. (1), this assuming $R_T = 30$ kΩ and $\dot{v} \sim 2f$, the exact prefactor of the latter depending on the waveform, and proportional to driving amplitude and island charging energy. For even smaller errors, one needs to consider lower temperatures or alternative superconductors with larger gap. Practical errors in the bolometric detection are two-fold. The ones related to efficiency of the N trap at low T vanish as $1 - \eta \propto T^{-5} e^{-\Delta/k_B T}$ according to Eq. (8), meaning that this error is $\ll 1\%$ even at $T < 150$ mK, and thus fully manageable. As a last point we note that the fundamental noise in measuring the temperature of the absorber is dictated by the thermal electron-phonon noise power given near equilibrium by the fluctuation-dissipation theorem as $S_{\dot{Q}} = 10\Sigma_N \mathcal{V}_N k_B T^6$ [23]. Signal-to-noise ratio is then $2f\Delta/\sqrt{S_{\dot{Q}}\nu}$ with measurement bandwidth ν. With typical parameters, this yields a value $\approx 10^5$ for $f = 100$ MHz, $\nu = 1$ Hz and $T = 100$ mK. Therefore, the accuracy of the frequency-to-power conversion is not limited fundamentally by the bolometric detection.

In summary, the main fundamental errors in frequency-to-power conversion stem from nonvanishing temperature $(\frac{1}{2} k_B T/\Delta)$, and from nonvanishing operation frequency [in a real setup $\propto (R_T f/\Delta)^{2/3}$]. The junction quality via the subgap leakage poses another limitation with error vanishing exponentially with the "hardness" of the gap. Here, we have analyzed a BCS superconductor as the energy filter; similar analysis could be done for other types of emitters such as single-level quantum dots. Finally, we believe that the present error analysis can possibly be complemented by pumping error accounting [24].

We thank Dmitry Golubev for many useful discussions. This work was supported by Academy of Finland (Grant No. 312057).

[1] M.-H. Bae, D.-H. Chae, M.-S. Kim, B.-K. Kim, S.-I. Park, J. Song, T. Oe, N.-H. Kaneko, N. Kim, and W.-S. Kim, Metrologia **57**, 065025 (2020).
[2] H. Scherer and B. Camarota, Meas. Sci. Technol. **23**, 124010 (2012).
[3] S. P. Giblin, E. Mykkänen, A. Kemppinen, P. Immonen, A. Manninen, M. Jenei, M. Möttönen, G. Yamahata, A. Fujiwara, and M. Kataoka, Metrologia **57**, 025013 (2020).
[4] I. Y. Krasnopolin, R. Behr, and J. Niemeyer, Supercond. Sci. Technol. **15**, 1034 (2002).
[5] R. Ribeiro-Palau *et al.*, Nat. Nanotechnol. **10**, 965 (2015).
[6] C. Bäuerle, D. C. Glattli, T. Meunier, F. Portier, P. Roche, P. Roulleau, S. Takada, and X. Waintal, Rep. Prog. Phys. **81**, 056503 (2018).
[7] M. Carrega, L. Chirolli, S. Heun, and L. Sorba, Nat. Rev. Phys. **3**, 698 (2021).
[8] M. Marín-Suárez, J. T. Peltonen, D. S. Golubev, and J. P. Pekola, Nat. Nanotechnol. **17**, 239 (2022).
[9] V. Kashcheyevs, Nat. Nanotechnol. **17**, 225 (2022).
[10] See Supplemental Material at http://link.aps.org/supplemental/10.1103/PhysRevLett.129.037702 for a schematic of the initial proposal, description of the injector numerics, and material parameters used in the heat transport calculation, which includes Refs. [11,12].
[11] D. V. Averin and J. P. Pekola, Phys. Rev. Lett. **101**, 066801 (2008).
[12] V. F. Maisi, Doctoral thesis, Aalto University, School of Science, 2014, http://urn.fi/URN:ISBN:978-952-6682-11-2.
[13] J. Bardeen, L. N. Cooper, and J. R. Schrieffer, Phys. Rev. **108**, 1175 (1957).
[14] F. C. Wellstood, C. Urbina, and J. Clarke, Phys. Rev. B **49**, 5942 (1994).
[15] J. N. Ullom, P. A. Fisher, and M. Nahum, Phys. Rev. B **61**, 14839 (2000).
[16] J. N. Ullom, P. A. Fisher, and M. Nahum, Phys. Rev. B **58**, 8225 (1998).
[17] R. C. Dynes, V. Narayanamurti, and J. P. Garno, Phys. Rev. Lett. **41**, 1509 (1978).
[18] R. C. Dynes, J. P. Garno, G. B. Hertel, and T. P. Orlando, Phys. Rev. Lett. **53**, 2437 (1984).
[19] Bayan Karimi, Yu-Cheng Chang, and Jukka P. Pekola, J. Low Temp. Phys. **207**, 220 (2022).
[20] J. Bardeen, G. Rickayzen, and L. Tewordt, Phys. Rev. **113**, 982 (1959).
[21] V. F. Maisi, S. V. Lotkhov, A. Kemppinen, A. Heimes, J. T. Muhonen, and J. P. Pekola, Phys. Rev. Lett. **111**, 147001 (2013).
[22] J. P. Pekola, V. F. Maisi, S. Kafanov, N. Chekurov, A. Kemppinen, Y. A. Pashkin, O. P. Saira, M. Mottonen, and J. S. Tsai, Phys. Rev. Lett. **105**, 026803 (2010).
[23] B. Karimi, F. Brange, P. Samuelsson, and J. P. Pekola, Nat. Commun. **11**, 367 (2020).
[24] D. Reifert, M. Kokainis, A. Ambainis, V. Kashcheyevs, and Niels Ubbelohde, Nat. Commun. **12**, 285 (2021).

Correction: A sign error in Eq. (5) has been fixed.